Stabilized Predictor-Corrector Schemes for Gradient Flows with Strong Anisotropic Free Energy

Jie Shen[1] and Jie Xu[1,*]

[1] *Department of Mathematics, Purdue University, USA.*

Abstract. Gradient flows with strong anisotropic free energy are difficult to deal with numerically with existing approaches. We propose a stabilized predictor-corrector approach to construct schemes which are second-order accurate, easy to implement, and maintain the stability of first-order stabilized schemes. We apply the new approach to three different type of gradient flows with strong anisotropic free energy: anisotropic diffusion equation, anisotropic Cahn-Hilliard equation, and Cahn-Hilliard equation with degenerate diffusion mobility. Numerical results are presented to show that the stabilized predictor-corrector schemes are second-order accurate, unconditionally stable for the first two equations, and allow larger time step than the first-order stabilized scheme for the last equation. We also prove rigorously that, for the isotropic Cahn-Hilliard equation, the stabilized predictor-corrector scheme is of second-order.

1 Introduction

Many dynamical physical processes can be described by gradient flows of the governing free energy (see for example [1–6]). When dealing with strongly anisotropic systems, the gradient flows are usually characterized by nonlinear couplings of spatial derivatives. We mention some examples here, including concentration-dependent diffusion mobility [7,8] or elasticity [9], and anisotropic interfacial energy [10–12].

From the computational perspective, it is crucial to construct energy stable numerical schemes. There are several different techniques to construct energy stable schemes, including convex splitting [13,14], stabilization [15,16], invariant energy quadratization (IEQ) [9,17–19] and the newly introduced scalar auxiliary variable (SAV) approach [20].

However, for gradient flows with strong anisotropic free energy, it is difficult to construct robust second-order schemes using these approaches as we explain below. The convex splitting and stabilization approaches usually lead to only first-order schemes, although second-order schemes are available for certain special cases without nonlinear derivative terms. One can formally construct second-order energy stable schemes using IEQ or SAV approach as long as one can split the free energy into two terms, one is a linear quadratic term and the other is bounded from below. But we may not be able to do so with free energies having strong nonlinear derivative terms. Furthermore, the stability of IEQ and SAV is with respect to a modified energy which, in cases of strong nonlinear derivative terms, may not a good approximation of the original energy, could lead to non-physical oscillations [20].

In this work, we construct second-order stabilized predictor-corrector scheme for gradient flows with strongly nonlinear couplings of spatial derivatives. More precisely, we use the first-order stabilized scheme as the predictor, followed by a second-order corrector step. The scheme enjoys the following advantages:

- Simplicity: it only requires solving linear equations with constant coefficients at each time step.

- Stability: we shall show numerically that it is at least as stable as the first-order stabilized scheme.

- Accuracy: we shall show, analytically for a simple case and numerically with extensive examples, that the scheme is second-order accurate.

We shall consider three different types of gradient flows with strong anisotropic free energy, and construct stabilized predictor-corrector schemes for each case. First, we consider in Section 2 an anisotropic diffusion equation, and introduce the stabilized predictor-corrector approach. As a comparison, we also consider the second-order Crank-Nicolson scheme with Adam-Bashforth extrapolation for nonlinear terms. We will show that the stabilized predictor-corrector approach is much more robust than the Crank-Nicolson scheme with Adam-Bashforth extrapolation. We then apply the stabilized predictor-corrector approach to a strongly anisotropic Cahn-Hilliard equation in Section 3 and to the Cahn-Hilliard equation with degenerate diffusion mobility in Section 4. In all cases, our numerical results indicate that the stabilized predictor-corrector schemes are second-order accurate while having good stability. Finally, we carry out a rigorous error analysis in Section 5 to show the second-order convergence for the isotropic Cahn-Hilliard equation.

2   Anisotropic diffusion equation

In order to motivate the stabilized predictor-corrector approach, we consider in this section the following free energy functional,

$$F[\phi] = \frac{1}{2} \int \mathrm{d}\boldsymbol{x} a(\phi) |\nabla \phi|^2, \tag{2.1}$$

where we assume that a is bounded and non-negative. Such free energy can be found in many applications, e.g., as part of the free energy in the Cahn-Hilliard equation with anisotropic interfacial energy considered in the next section.

We examine the L^2 gradient flow

$$\phi_t = \nabla \cdot (a(\phi) \nabla \phi) - \frac{1}{2} |\nabla \phi|^2 a'(\phi). \tag{2.2}$$

If a is constant, it reduces to the heat equation. We are interested in the case where $a_{\max}/a_{\min}$ is very large or even unbounded, which brings difficulty in solving the equation numerically.

One widely used strategy to construct stabilized schemes is to split the free energy $F = F_1 - F_2$ with

$$F_1[\phi] = \frac{1}{2} \int \mathrm{d}\boldsymbol{x} \lambda |\nabla \phi|^2, \quad F_2[\phi] = \frac{1}{2} \int \mathrm{d}\boldsymbol{x} (\lambda - a) |\nabla \phi|^2, \tag{2.3}$$

where $\lambda > a_{\max}$. Then, a first-order semi-implicit stabilized scheme is given by

$$\begin{aligned}
\frac{\phi^{n+1} - \phi^n}{\Delta t} &= -\frac{\delta F_1}{\delta \phi} [\phi^{n+1}] + \frac{\delta F_2}{\delta \phi} [\phi^n] \\
&= \lambda \Delta \phi^{n+1} - \nabla \cdot ((\lambda - a(\phi^n)) \nabla \phi^n) - \frac{1}{2} |\nabla \phi^n|^2 a'(\phi^n).
\end{aligned} \tag{2.4}$$

The above scheme is proven to be very stable but has large splitting errors. To increase the accuracy, we can consider the following second-order Crank-Nicolson Adam-Bashforth scheme:

$$\begin{aligned}
\frac{\phi^{n+1} - \phi^n}{\Delta t} &= -\frac{\delta F_1}{\delta \phi} [\frac{1}{2}(\phi^{n+1} + \phi^n)] + \frac{\delta F_2}{\delta \phi} [\bar{\phi}^{n+1/2}] \\
&= \frac{\lambda}{2} \Delta(\phi^{n+1} + \phi^n) - \nabla \cdot ((\lambda - a(\bar{\phi}^{n+1/2})) \nabla \bar{\phi}^{n+1/2}) - \frac{1}{2} |\nabla \bar{\phi}^{n+1/2}|^2 a'(\bar{\phi}^{n+1/2}),
\end{aligned} \tag{2.5}$$

with

$$\bar{\phi}^{n+1/2} = (3\phi^n - \phi^{n-1})/2. \tag{2.6}$$

However, numerical experiments indicate that the above scheme is not very robust at larger time steps, particularly when anisotropy is strong and the initial condition has large derivatives. In order to construct a more robust and efficient second-order scheme, we propose to use a predictor-corrector approach. More precisely, instead of using
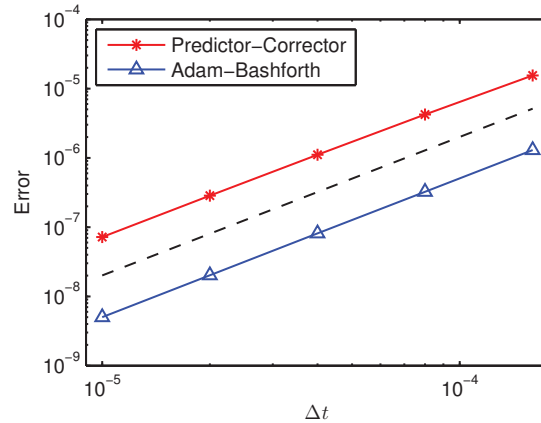
Fig. 1: Errors of predictor-corrector scheme and Adam-Bashforth scheme for (2.2) with the initial condition (2.8). The dashed line is the reference of the second-order convergence.

$\bar{\phi}^{n+1/2} = (3\phi^n - \phi^{n-1})/2$ in (2.5), we compute it by using the first-order scheme (2.4) at $t^{n+1/2}$, i.e., we determine $\bar{\phi}^{n+1/2}$ from

$$\frac{\bar{\phi}^{n+1/2} - \phi^n}{\Delta t/2} = \lambda \Delta \bar{\phi}^{n+1/2} - \nabla \cdot ((\lambda - a(\phi^n))\nabla \phi^n) - \frac{1}{2}|\nabla \phi^n|^2 a'(\phi^n). \qquad (2.7)$$

We shall show, with ample numerical results, that the predictor-corrector scheme (2.5) with (2.7) performs much better than the Crank-Nicolson Adam-Bashforth scheme (2.5) with (2.6). An intuitive explanation is that the first-order predictor is able to suppress high-frequency oscillations, while the Adam-Bashforth extrapolation can not.

We first examine the accuracy of the predictor-corrector scheme and the second-order Crank-Nicolson Adam-Bashforth scheme. We set $a(\phi) = 1 + 0.8\sin\phi$, $\Omega = [0,2\pi]^2$ with periodic boundary conditions, and take the initial condition to be

$$\phi(x,y,0) = 2\cos(2x+y) + \cos(x-2y). \qquad (2.8)$$

The space is discretized by $2^7 \times 2^7$ using Fourier-spectral methods. The numerical errors for both schemes at $T = 0.16$ are plotted in Fig. 1. We observe that both schemes are second-order accurate but the errors of Adam-Bashforth scheme are slightly smaller. But as we shall see below, this slight loss of accuracy will be more than compensated by its excellent stability.

Next, we compare the stability of the predictor-corrector scheme and the Crank-Nicolson Adam-Bashforth scheme. We choose a strongly disparate coefficient $a(\phi) = 1 + 0.99\sin\phi$ with the initial condition

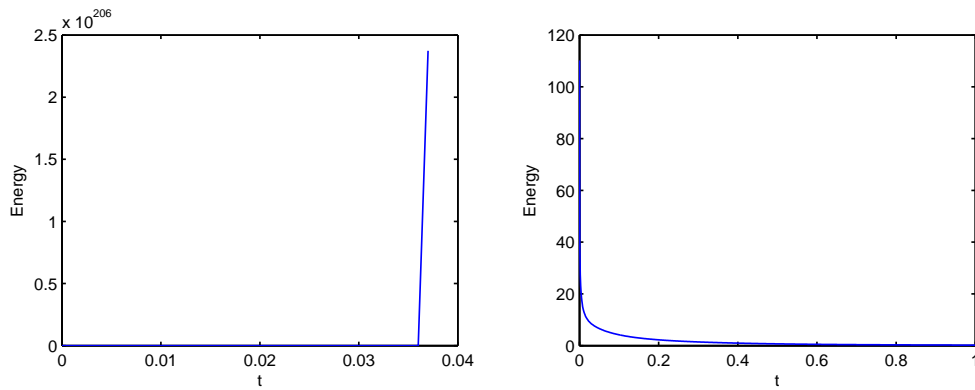$$\phi(x,y,0) = \frac{3}{\pi}\arctan\left(\frac{(x-\pi)^2 + (y-\pi)^2 - (2\pi/2.56)^2}{0.05}\right).$$

Fig. 2: Energy as a function of the time for $a=1+0.99\sin\phi$, where $\Delta t=10^{-3}$. Left: Adam-Bashforth. Right: Predictor-corrector.
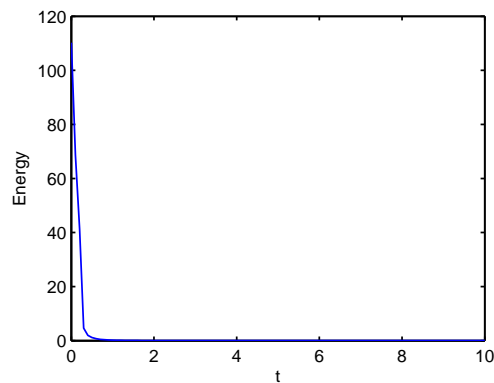

Fig. 3: Energy as a function of the time for $a=1+0.9999\sin\phi$, where $\Delta t=0.1$.

We choose $\Delta t=10^{-3}$ with $2^9\times 2^9$ spatial resolution to adequately resolve the arctan function. The energy evolutions of both schemes are plotted in Fig. 2. The Crank-Nicolson Adam-Bashforth scheme quickly blows up, while the predictor-corrector scheme keeps the energy dissipation. To further demonstrate the robustness of the predictor-corrector scheme, we test the predictor-corrector scheme with an even more disparate coefficient $a(\phi)=1+0.9999\sin\phi$, and a much larger time step $\Delta t=0.1$, The energy of the predictor-corrector scheme is plotted in Fig. 3, which indicates that the method still works very well.

From these examples, we can see that the predictor-corrector scheme achieves the second order accuracy while maintaining good stability. This is particularly useful when there is strong nonlinearity in derivatives and when the coefficients are nearly degenerate.

To further demonstrate the robustness of the predictor-corrector approach, we will apply the predictor-corrector approach to two challenging phase-field type equations.

3 Cahn-Hilliard equation with anisotropic interfacial energy

We consider in this section the anisotropic Cahn-Hilliard equation, a phase-field model that describes binary mixture with anisotropic interfacial energy [10–12,21], with the free energy in the following form

$$F[\phi] = \int d\mathbf{x} \left(\frac{1}{\epsilon^2} f(\phi) + \frac{\gamma(\mathbf{n})}{2} |\nabla \phi|^2 + \frac{\beta}{2} \omega^2 \right), \tag{3.1}$$

where $\mathbf{n} = \nabla \phi / |\nabla \phi|$ is the unit vector along $\nabla \phi$ (the unit vector normal to the interface), and $f(\phi) = (1 - \phi^2)^2 / 4$. The interfacial free energy density $\gamma(\mathbf{n})$ is given by

$$\gamma(\mathbf{n}) = 1 + a \left(4 \sum_i n_i^4 - 3 \right), \tag{3.2}$$

In the 2D case, it can also be written as $\gamma(\mathbf{n}) = 1 + a\cos(4\theta)$, where θ is the orientational angle of $\mathbf{n}$. The last term in the free energy is the regularization term for the case of strong anisotropy (when a is large),

$$\omega = \frac{\kappa}{\epsilon^2} f'(\phi) - \Delta \phi. \tag{3.3}$$

In the above, κ may take two values 0 or 1. When $\kappa = 0$, it is the bi-Laplacian regularization; when $\kappa = 1$, it is the Willmore regularization. Then, the H^{-1} gradient flow with this free energy is

$$\phi_t = \Delta \frac{\delta F}{\delta \phi}, \tag{3.4}$$

where

$$\begin{aligned}
\frac{\delta F}{\delta \phi} &= \frac{1}{\epsilon^2} f'(\phi) + \beta \left(\kappa \frac{f''(\phi)}{\epsilon^2} - \Delta \right) \left(\kappa \frac{f'(\phi)}{\epsilon^2} - \Delta \phi \right) \\
&\quad - \nabla \cdot (\gamma(\mathbf{n}) \nabla \phi) - \frac{1}{2} \partial_i \left(|\nabla \phi| (\delta_{ij} - n_i n_j) \partial_{n_j} \gamma(\mathbf{n}) \right),
\end{aligned}$$

with the Einstein summation convention in the last term.

The about equation is notoriously difficult to solve since it involves sixth order derivatives with strong nonlinear coupling. A first-order nonlinear scheme was proposed in [11], while a linear stabilized first-order scheme was proposed in [12]. Due to the strong nonlinear coupling, no second-order scheme is available. We propose below a second-order predictor-corrector scheme based on the first order stabilized scheme.

3.1 Numerical scheme

We split the free energy $F = F_1 - F_2$ with

$$F_1[\phi] = \frac{\beta}{2}\|\Delta\phi\|^2 + \frac{\kappa\beta S_2 + M\epsilon^2}{2\epsilon^2}\|\nabla\phi\|^2 + \frac{\kappa\beta S_1 + S_0\epsilon^2}{2\epsilon^4}\|\phi\|^2, \tag{3.5}$$

$$F_2[\phi] = \frac{1}{\epsilon^2}\Big[\frac{S_0}{2}\|\phi\|^2 - (f(\phi),1)\Big] + \frac{M - \gamma(\boldsymbol{n})}{2}\|\nabla\phi\|^2$$
$$+ \frac{\kappa\beta S_1}{2\epsilon^4}\|\phi\|^2 + \frac{\kappa\beta S_2}{2\epsilon^2}\|\nabla\phi\|^2 + \frac{\beta}{2}\|\Delta\phi\|^2 - \frac{\beta}{2}\Big\|\kappa\frac{f'(\phi)}{\epsilon^2} - \Delta\phi\Big\|^2. \tag{3.6}$$

In the above, we introduced four stabilizing constants S_0, S_1, S_2, M. Intuitively, they shall be chosen such that F_1 and F_2 are at least positive definite. Then, a first-order stabilized scheme can be constructed by dealing with F_1 implicitly and F_2 explicitly, namely:

$$\frac{\phi^{n+1} - \phi^n}{\Delta t} = \Delta\mu^{n+1}, \tag{3.7}$$

$$\mu^{n+1} = \beta\Delta^2\phi^{n+1} + \frac{1}{\epsilon^2}\Big(S_0(\phi^{n+1} - \phi^n) + f'(\phi^n)\Big)$$
$$- M\Delta(\phi^{n+1} - \phi^n) - \nabla\cdot(\gamma(\boldsymbol{n}^n)\nabla\phi^n) - \frac{1}{2}\partial_i\Big(|\nabla\phi^n|(\delta_{ij} - n_i^n n_j^n)\partial_{n_j}\gamma(\boldsymbol{n}^n)\Big)$$
$$+ \kappa\frac{\beta}{\epsilon^4}\Big(S_1(\phi^{n+1} - \phi^n) + f'(\phi^n)f''(\phi^n)\Big)$$
$$- \kappa\frac{\beta}{\epsilon^2}\Big(S_2\Delta(\phi^{n+1} - \phi^n) + \Delta f'(\phi^n) + f''(\phi^n)\Delta\phi^n\Big). \tag{3.8}$$

The second-order predictor-corrector scheme is written as

$$\frac{\phi^{n+1} - \phi^n}{\Delta t} = \Delta\mu^{n+1/2}, \tag{3.9}$$

$$\mu^{n+1/2} = \beta\Delta^2\frac{1}{2}(\phi^{n+1} + \phi^n) + \frac{1}{\epsilon^2}\Big(S_0\big(\frac{1}{2}(\phi^{n+1} + \phi^n) - \bar{\phi}^{n+1/2}\big) + f'(\bar{\phi}^{n+1/2})\Big)$$
$$- M\Delta\Big(\frac{1}{2}(\phi^{n+1} + \phi^n) - \bar{\phi}^{n+1/2}\Big) - \nabla\cdot(\gamma(\boldsymbol{n}^{n+1/2})\nabla\bar{\phi}^{n+1/2})$$
$$- \frac{1}{2}\partial_i\Big(|\nabla\bar{\phi}^{n+1/2}|(\delta_{ij} - n_i^{n+1/2}n_j^{n+1/2})\partial_{n_j}\gamma(\boldsymbol{n}^{n+1/2})\Big)$$
$$+ \kappa\frac{\beta}{\epsilon^4}\Big(S_1\big(\frac{1}{2}(\phi^{n+1} + \phi^n) - \bar{\phi}^{n+1/2}\big) + f'(\bar{\phi}^{n+1/2})f''(\bar{\phi}^{n+1/2})\Big)$$
$$- \kappa\frac{\beta}{\epsilon^2}\Big(S_2\Delta\big(\frac{1}{2}(\phi^{n+1} + \phi^n) - \bar{\phi}^{n+1/2}\big) + \Delta f'(\bar{\phi}^{n+1/2}) + f''(\bar{\phi}^{n+1/2})\Delta\bar{\phi}^{n+1/2}\Big), \tag{3.10}$$

with $\bar{\phi}^{n+1/2}$ being obtained from ϕ^n using the first-order stabilized scheme (3.8) with the time step $\Delta t/2$.

3.2   Numerical examples

We consider (3.4) with the periodic boundary conditions in the domain $[0,L]\times[0,L)$ with $L=2$. The space is discretized by the Fourier spectral method with $2^8\times 2^8$ modes. The stabilization parameters are chosen as $M=S_0=S_1=S_2=8$. When showing the result, we draw the contour $\phi=0$ to represent the interface.

3.2.1   Accuracy and stability test

We choose $\epsilon=0.2$, $a=0.2$, $\beta=5\times10^{-4}$, and a smooth initial condition

$$\phi(0,x,y)=0.5\sin(\pi x)\sin(\pi y). \tag{3.11}$$

We plot the numerical error at $t=10^{-5}$ with different time steps in Fig. 4. The reference solution is the numerical solution with $\Delta t=5\times10^{-10}$. For both bi-Laplacian and Willmore regularization, we observe the second-order convergence.
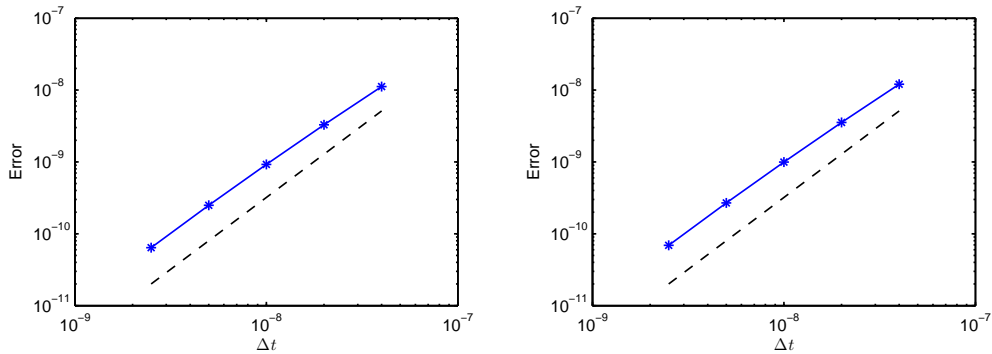

Fig. 4: Numerical errors by the scheme (3.10): The dashed lines are reference lines of second-order convergence. Left: bi-Laplacian regularization. Right: Willmore regularization.

Next we examine the stability of (3.10) with large time step. We choose a small $\epsilon=0.02$, a large anisotropic parameter $a=0.99$, and $\beta=5\times10^{-4}$. The initial condition is chosen as

$$\phi(0,x,y)=\tanh\left(\frac{\sqrt{(x-0.4L)^2+(y-0.51L)^2}-L/4}{\epsilon}\right)$$
$$+\tanh\left(\frac{\sqrt{(x-5L/6)^2+(y-0.49L)^2}-L/10}{\epsilon}\right)-1. \tag{3.12}$$

We use $\Delta t=10^{-2}$. The free energy and interfacial profiles at steady states are shown in Fig. 5. The energy dissipation is maintained and the steady states are correct. We plot in Fig. 6 the vertical cross section along $y=1$, which shows no high-frequency oscillation. We have also tried with even larger time steps, the numerical solution is still energy stable without high-frequency oscillation, indicating that the predictor-corrector scheme has very good stability.
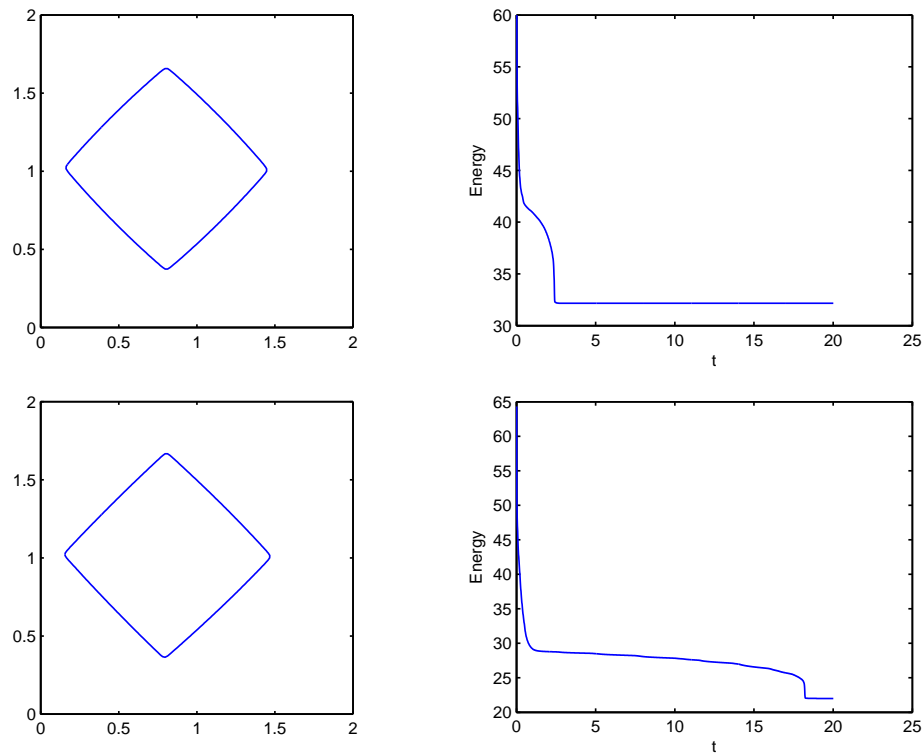
Fig. 5: Steady state and evolution of free energy when $a=0.99$ and $\Delta t=10^{-2}$. Top: bi-Laplacian regularization. Bottom: Willmore regularization.
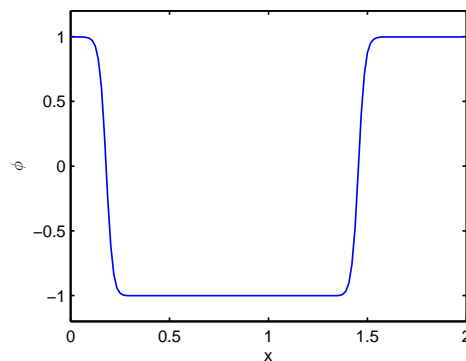

Fig. 6: The profile of ϕ on $y=1$ in Fig. 5 bottom.

3.2.2 Roughing process of a smooth curve

Here, we examine evolution of a smooth interface to facets. We adopt the Willmore regularization and choose $\epsilon=0.02$, $a=0.8$, $\beta=4\times10^{-4}$, and the initial condition

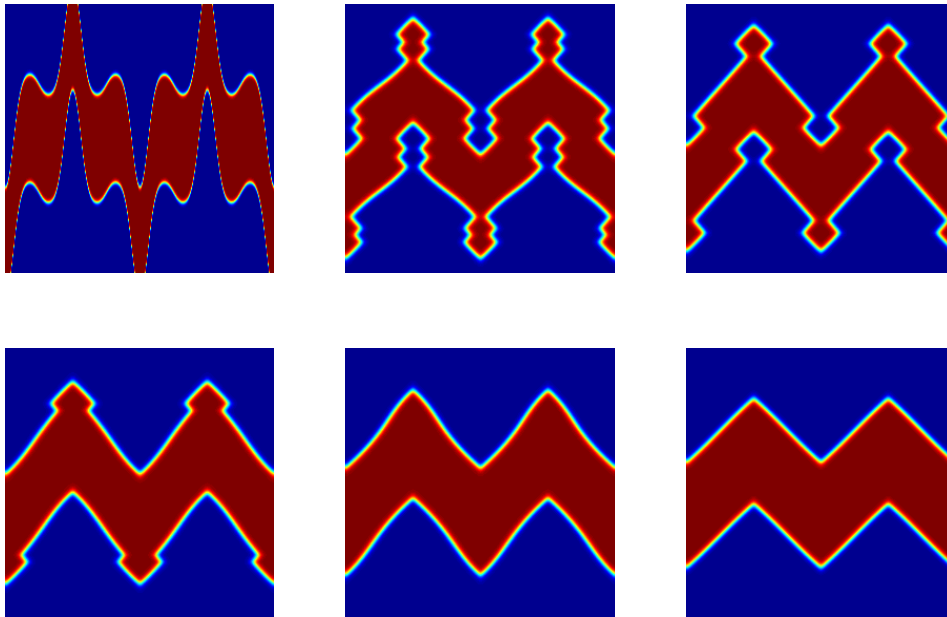$$\phi(x,y,0)=\tanh(-(y-0.7L-0.2r_1)/\epsilon)+\tanh((y-0.3L-0.2r_1)/\epsilon)-1, \qquad (3.13)$$

Fig. 7: Evolution of smooth interface to facets. From left to right: $t=k\times10^{-4}$ with $k=0,0.5,1$ (top) and $k=2,3,4$ (bottom).

where

$$r_1(x)=1.8\cos(4\pi x/L)+1.5\cos(12\pi x/L)+0.4\cos(20\pi x/L)+0.1\cos(28\pi x/L). \quad (3.14)$$

we take the time step to be $\Delta t=10^{-6}$. The configuration is shown in Fig. 7. We observe that an initially smooth interface quickly forms many small facets along the low-energy orientations, followed by combinations of small facets into large ones. These simulations are consistent with the results in [11,12].

3.2.3   Wulff shape of a droplet

We choose, as the initial data, a circular droplet

$$\phi(0,x,y)=\tanh\left(\frac{\sqrt{(x-0.5L)^2+(y-0.5L)^2}-L/4}{\epsilon}\right), \quad (3.15)$$

and examine the Wulff shape equilibrium state. We focus on the Willmore regularization and choose $\epsilon=0.02$. First we fix $\beta=4\times10^{-4}$ and examine the effect of the anisotropic parameter a (Fig. 8). As a increases, the facets become more flat and the corners become sharper. Then we fix $a=0.8$ and let β vary (Fig. 9). There is no visible difference with respect to the facets, but the corner is wider and smoother as β increases.
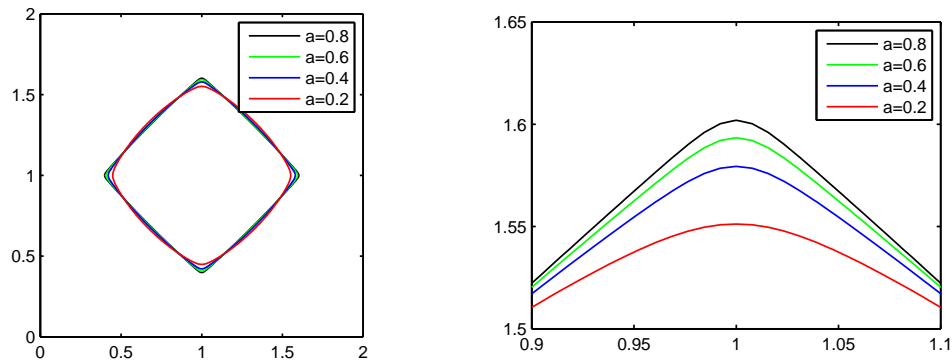
Fig. 8: The Wulff shape with different a. The right plot is the top corner of the left plot.
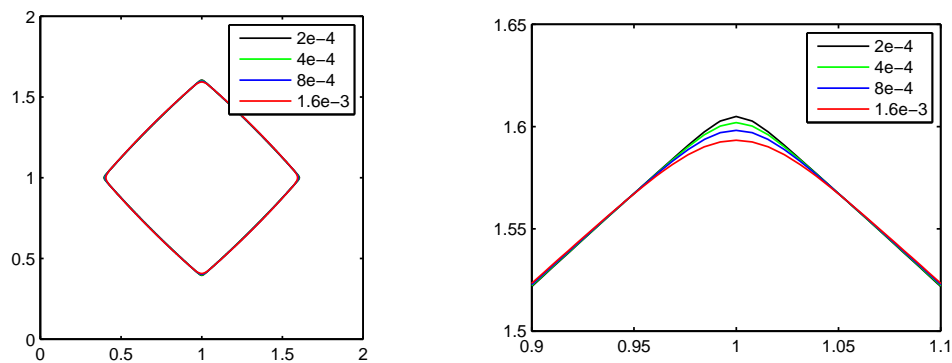

Fig. 9: The Wulff shape with different β. The right plot is the top corner of the left plot.

3.2.4 Coarsening dynamics

We fix $\epsilon = 0.02$, $\beta = 5 \times 10^{-4}$ and let the anisotropic parameter a vary. The initial condition is chosen as (3.12), and the time step is $\Delta t = 10^{-7}$. The interfacial profile and evolution of free energy are plotted in Fig. 10 for $a = 0.2$ and Fig. 11 for $a = 0.6$ for both bi-Laplacian and Willmore regularization. By looking at both the energy and the interfacial profile, we find that the coarsening process is faster when $a = 0.2$. Besides, with bi-Laplacian regularization the coarsening process is also faster than the Willmore regularization. This is possibly because the bi-Laplacian introduce addition dissipation throughout the domain, but Willmore only within the interfacial layer. For the Willmore regularization with $a = 0.6$, the two droplets first merge into one, then the shape evolves to the Wulff shape. For the other three cases, the two droplets first evolve into a Wulff shape, then the coarsening process takes place. To see this more clearly, we also plot ϕ at $y = 0.9375$ in Fig. 12 for Willmore regularization.
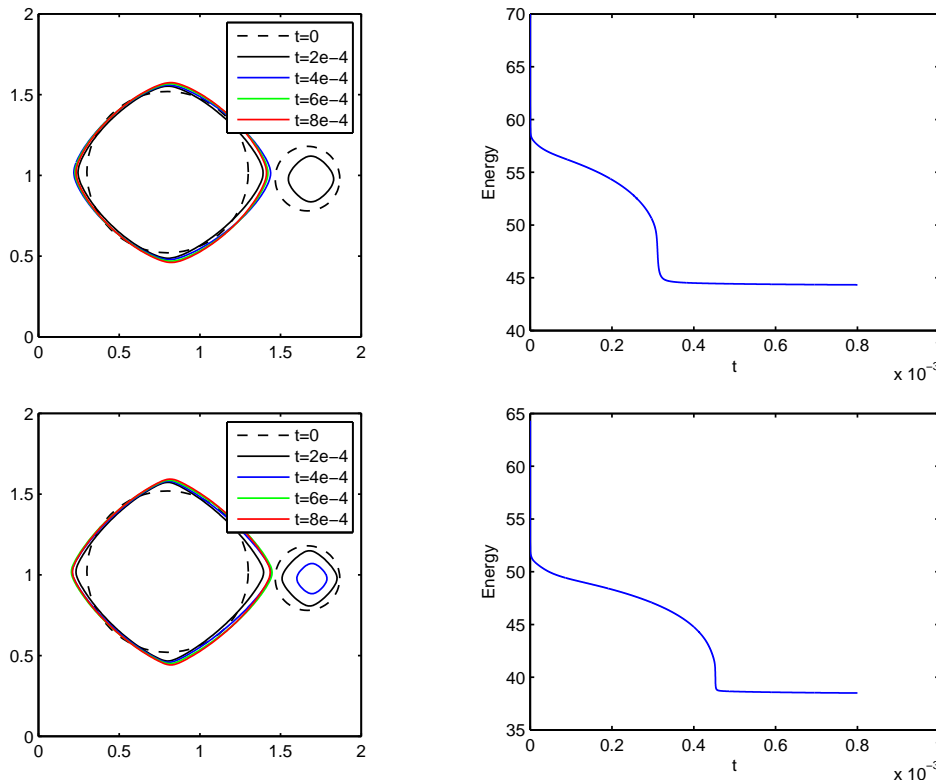
Fig. 10: Evolution of free energy and interface when $a=0.2$. Top: bi-Laplacian regularization. Bottom: Willmore regularization.

4   Cahn-Hilliard equation with degenerate diffusion mobility

We consider the isotropic free energy

$$F[\phi] = \int \mathrm{d}x \left(\frac{1}{\epsilon^2} f(\phi) + \frac{1}{2} |\nabla \phi|^2 \right), \tag{4.1}$$

where $f(\phi) = (1-\phi^2)^2/4$, with a variable diffusive mobility $M(\phi) = |1-\phi^2|$. The H^{-1} gradient flow, with the variable mobility, is given by

$$\phi_t = \nabla \cdot \left(M(\phi) \nabla \left(-\Delta \phi + \frac{1}{\epsilon^2} f'(\phi) \right) \right). \tag{4.2}$$

It is observed that the constant mobility leads to dissipation in the whole domain, while this variable mobility restrains the dissipation inside the interface layer [7,8].
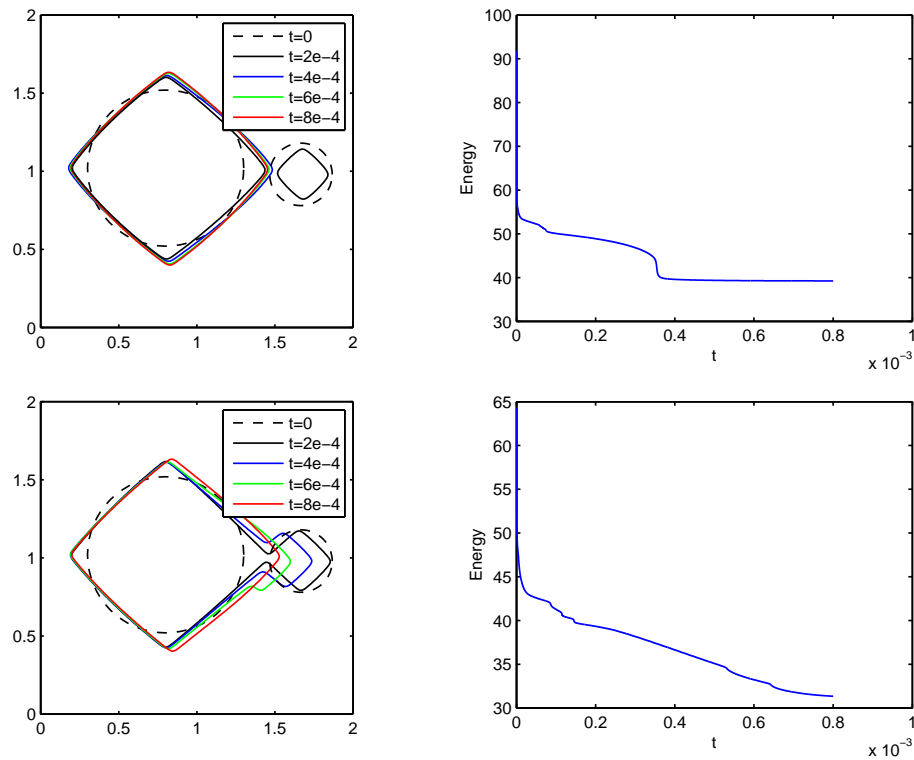
Fig. 11: Evolution of free energy and interface when $a=0.6$. Top: bi-Laplacian regularization. Bottom: Willmore regularization.
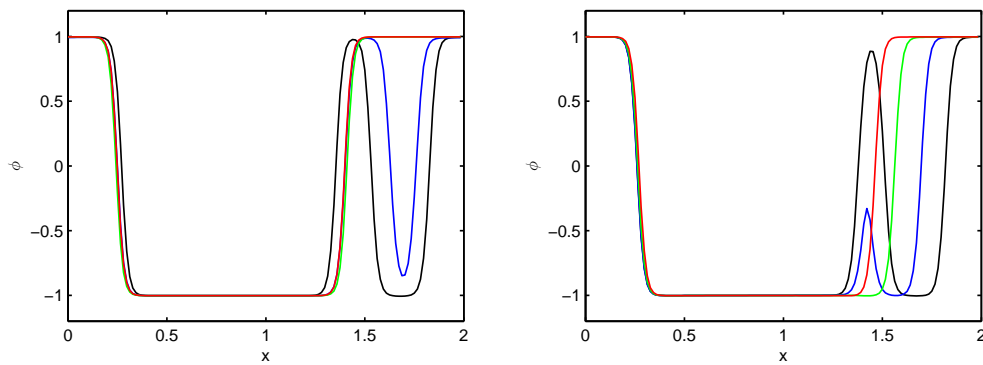

Fig. 12: Profiles of ϕ at $y=0.9375$ for the Willmore regularization. Left: $a=0.2$ (Fig. 10); Left: $a=0.6$ (Fig. 11).

4.1 Numerical schemes

We start from the first-order stabilized scheme used in [8]:

$$\frac{\bar{\phi}^{n+1}-\phi^n}{\Delta t}=-\lambda\Delta^2\bar{\phi}^{n+1}+\nabla\cdot\left((\lambda-M(\phi^n))\nabla\Delta\phi^n\right)+\nabla\cdot\left(M(\phi^n)\nabla\frac{1}{\epsilon^2}f'(\phi^n)\right), \qquad (4.3)$$

where λ is a suitable stabilizing parameter.

The second-order predictor-corrector scheme is then given by

$$\frac{\phi^{n+1}-\phi^n}{\Delta t}=-\frac{\lambda}{2}\Delta^2(\phi^{n+1}+\phi^n)$$

$$+\nabla\cdot\left((\lambda-M(\bar{\phi}^{n+1/2}))\nabla\Delta\bar{\phi}^{n+1/2}\right)+\nabla\cdot\left(M(\bar{\phi}^{n+1/2})\nabla\frac{1}{\epsilon^2}f'(\bar{\phi}^{n+1/2})\right), \quad (4.4)$$

where $\bar{\phi}^{n+1/2}$ is computed by (4.3) with the time step $\Delta t/2$.

Note that one should use a weak formulation in the implementation of both schemes (4.3) and (4.4) to avoid taking derivatives of $M(\bar{\phi}^{n+1/2})$. We point out that the semi-implicit scheme is energy stable only when the time step is not large. Thus we cannot expect the energy stability of the predictor-corrector scheme for large time step.

4.2 Numerical examples

We choose $\epsilon=0.02$ and consider the domain $[0,2)\times[0,2)$ with periodic boundary conditions. The space is discretized by $2^7\times2^7$ Fourier modes. The stabilization parameter is chosen as $\lambda=2$.

4.2.1 Accuracy and stability test

To check the accuracy, we choose a smooth initial condition

$$\phi(0,x,y)=0.5\sin(\pi x)\sin(\pi y). \quad (4.5)$$

We plot the numerical error at $t=4\times10^{-5}$ in Fig. 13. The reference solution is given by $\Delta t=10^{-9}$.
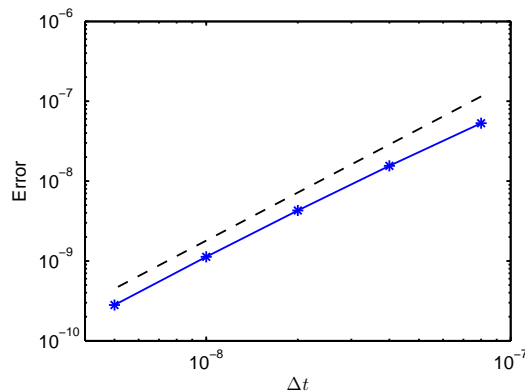

Fig. 13: Numerical error of the equation (4.2) at $t=4\times10^{-5}$. The dashed line is a reference of second-order convergence.
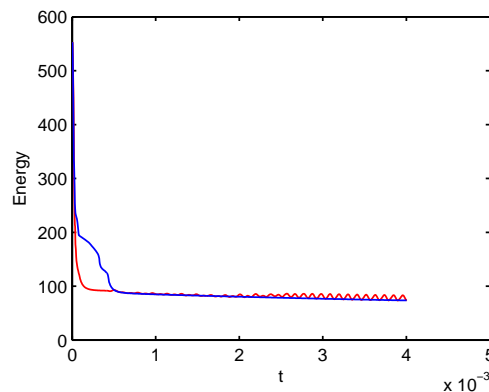
Fig. 14: Evolution of free energy with $\Delta t = 4 \times 10^{-6}$. Red: semi-implicit; blue: predictor-corrector.

As for the stability, we find that with $\Delta t = 10^{-5}$, both schemes blow up. With $\Delta t = 4 \times 10^{-6}$, the stabilized scheme exhibits oscillations in energy, while the predictor-corrector scheme keeps energy dissipation (see Fig. 14), indicating that the predictor-corrector scheme, not only is more accurate at second-order, but is also more stable.

4.2.2 Coarsening dynamics

We take the initial condition

$$\phi(0,x,y) = \tanh\left(\frac{\sqrt{(x-0.4L)^2 + (y-0.55L)^2} - L/4}{\epsilon}\right)$$
$$+ \tanh\left(\frac{\sqrt{(x-5L/6)^2 + (y-0.45L)^2} - L/10}{\epsilon}\right) - 1,$$

with $L = 2$ being the length of the domain. We choose $\Delta t = 4 \times 10^{-7}$. The contour $\phi = 0$ are plotted in Fig. 15 left. We also compare the energy evolutions with $M = |1 - \phi^2|$ and $M = 1$, plotted in Fig. 15 right. It is found that the coarsening is much slower with $M = |1 - \phi^2|$, which is consistent with the results in [7,8].

5   Error estimate of the isotropic Cahn-Hilliard equation

While it is clear that the predictor-corrector scheme used in this paper is second-order if applied to ordinary differential equations, it is not so clear under what conditions it will provide second-order accuracy for partial differential equations. We shall consider the isotropic Cahn-Hilliard equation

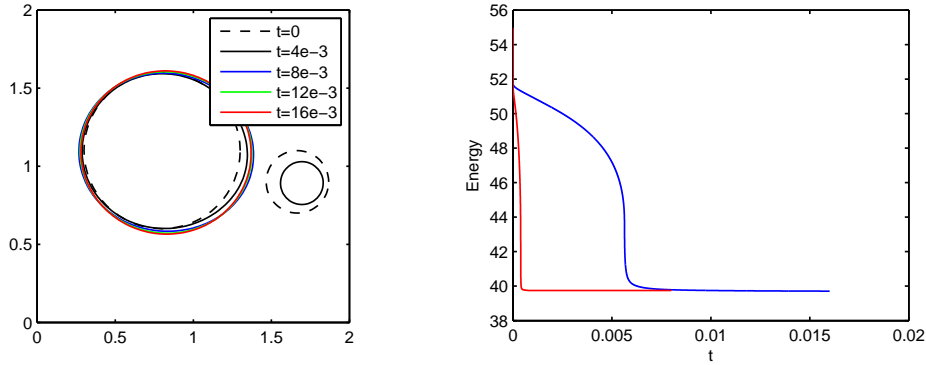$$\phi_t = \Delta(-\Delta\phi + f(\phi)), \tag{5.1}$$

Fig. 15: Left: evolution of interface with the mobility $M(\phi)=|1-\phi^2|$. Right: Free energy evolution with $M=1$ (red) and $M=|1-\phi^2|$ (blue).

and perform an error analysis for the predictor-corrector scheme

$$\frac{\bar{\phi}^{n+1/2}-\phi^n}{\Delta t/2}=\Delta\left(-\Delta\bar{\phi}^{n+1/2}+f(\phi^n)+S(\bar{\phi}^{n+1/2}-\phi^n)\right), \tag{5.2}$$

$$\frac{\phi^{n+1}-\phi^n}{\Delta t}=\Delta\left[-\frac{1}{2}\Delta(\phi^{n+1}+\phi^n)+f(\bar{\phi}^{n+1/2})+S\left(\frac{1}{2}(\phi^{n+1}+\phi^n)-\bar{\phi}^{n+1/2}\right)\right], \tag{5.3}$$

where S is a stabilizing constant.

Denote $e^n=\phi^n-\phi(t^n)$ and $\bar{e}^{n+1/2}=\bar{\phi}^{n+1/2}-\phi(t^{n+1/2})$.

Theorem 5.1. *Assuming that f satisfies the Lipchitz condition $|f(x)-f(y)|<L|x-y|$. For any $\Delta t<\left(1+4(L^2+S^2)\right)^{-1}$, there exists a constant C depending on L and S such that*

$$\|e^n\|^2\le C\exp\left(\left(1-(1+4(L^2+S^2))\Delta t\right)^{-1}t^n\right)\Delta t^4\int_0^{t^n}dt(\|\phi_t\|_{H^4}^2+\|\phi_{tt}\|_{H^2}^2+\|\phi_{ttt}\|^2). \tag{5.4}$$

Proof. We first give an estimate of $\bar{e}^{n+1/2}$. By comparing (5.2) with the equation at t^n, we deduce that

$$\frac{\bar{e}^{n+1/2}-e^n}{\Delta t/2}=\Delta\left[-\Delta\bar{e}^{n+1/2}+f(\phi^n)-f(\phi(t^n))+S(\bar{e}^{n+1/2}-e^n)\right]+\bar{T}^n, \tag{5.5}$$

where the truncation error $\bar{T}^n=\bar{T}_1^n+\bar{T}_2^n$ with

$$\bar{T}_1^n=\frac{\phi(t^{n+1/2})-\phi(t^n)}{\Delta t/2}-\phi_t(t^n)=-\frac{1}{\Delta t/2}\int_{t^n}^{t^{n+1/2}}dt(t-t^n)\phi_{tt},$$

$$\bar{T}_2^n=-\Delta^2\left(\phi(t^{n+1/2})-\phi(t^n)\right)+S\Delta\left(\phi(t^{n+1/2})-\phi(t^n)\right)=(-\Delta^2+S\Delta)\int_{t^n}^{t^{n+1/2}}dt\,\phi_t.$$

It is easy to see that we have

$$\|\bar{T}_1^n\|^2 \le C\Delta t \int_{t^n}^{t^{n+1/2}} \mathrm{d}t \, \|\phi_{tt}\|^2, \quad \|\bar{T}_2^n\|^2 \le C\Delta t \int_{t^n}^{t^{n+1/2}} \mathrm{d}t \, \|\phi_t\|_{H^4}^2.$$

Taking the inner product of (5.5) with $\bar{e}^{n+1/2}$, we obtain

$$\frac{1}{\Delta t}(\|\bar{e}^{n+1/2}\|^2 - \|e^n\|^2 + \|\bar{e}^{n+1/2} - e^n\|^2) + \|\Delta\bar{e}^{n+1/2}\|^2 + S\|\nabla\bar{e}^{n+1/2}\|^2$$

$$= \left(\Delta\bar{e}^{n+1/2}, f(\phi^n) - f(\phi(t^n)) - Se^n\right) + (\bar{e}^{n+1/2}, \bar{T}^n)$$

$$\le \|\Delta\bar{e}^{n+1/2}\|^2 + \frac{1}{4}\|f(\phi^n) - f(\phi(t^n)) - Se^n\|^2 + \frac{1}{4\Delta t}\|\bar{e}^{n+1/2}\|^2 + \Delta t\|\bar{T}_1^n + \bar{T}_2^n\|^2$$

$$\le \|\Delta\bar{e}^{n+1/2}\|^2 + \frac{1}{2}\|f(\phi^n) - f(\phi(t^n))\|^2 + \frac{S}{2}\|e^n\|^2 + \frac{1}{4\Delta t}\|\bar{e}^{n+1/2}\|^2 + 2\Delta t(\|\bar{T}_1^n\|^2 + \|\bar{T}_2^n\|^2)$$

$$\le \|\Delta\bar{e}^{n+1/2}\|^2 + \frac{L^2 + S^2}{2}\|e^n\|^2 + \frac{1}{4\Delta t}\|\bar{e}^{n+1/2}\|^2 + 2\Delta t(\|\bar{T}_1^n\|^2 + \|\bar{T}_2^n\|^2).$$

Together with $\Delta t \le 1/(L^2 + S^2)$, we arrive at

$$\|\bar{e}^{n+1/2}\|^2 \le \left(\frac{4}{3} + \frac{2(L^2 + S^2)}{3}\Delta t\right)\|e^n\|^2 + C\Delta t^3 \int_{t^n}^{t^{n+1/2}} \mathrm{d}t\,(\|\phi_{tt}\|^2 + \|\phi_t\|_{H^4}^2)$$

$$\le 2\|e^n\|^2 + C\Delta t^3 \int_{t^n}^{t^{n+1/2}} \mathrm{d}t\,(\|\phi_{tt}\|^2 + \|\phi_t\|_{H^4}^2). \tag{5.6}$$

Now we can estimate e^{n+1}. Comparing (5.3) with the equation at $t^{n+1/2}$, we deduce

$$\frac{e^{n+1} - e^n}{\Delta t} = \Delta\left[-\frac{1}{2}\Delta(e^{n+1} + e^n) + \left(f(\bar{\phi}^{n+1/2}) - f(\phi(t^{n+1/2}))\right)\right.$$

$$\left. + \frac{S}{2}(e^{n+1} + e^n - 2\bar{e}^{n+1/2})\right] + T_1^n + \Delta T_2^n. \tag{5.7}$$

The local truncation errors become

$$T_1^n = \frac{\phi(t^{n+1}) - \phi(t^n)}{\Delta t} - \phi_t(t^{n+1/2}) = \frac{1}{\Delta t}\int_{t^n}^{t^{n+1}} \mathrm{d}t \, \frac{1}{2}(t - t^{n+1/2})^2 \phi_{ttt},$$

$$T_2^n = -\frac{1}{2}\Delta\left(\phi(t^{n+1}) + \phi(t^n) - 2\phi(t^{n+1/2})\right) + \frac{S}{2}\left(\phi(t^{n+1}) + \phi(t^n) - 2\phi(t^{n+1/2})\right)$$

$$= (-\Delta + S)\int_{t^n}^{t^{n+1}} \mathrm{d}t\,(t - t^{n+1/2})\phi_{tt}.$$

Now the estimates for them are given by

$$\|T_1^n\|^2 \le C\Delta t^3 \int_{t^n}^{t^{n+1/2}} \mathrm{d}t\,\|\phi_{ttt}\|^2, \quad \|T_2^n\|^2 \le C\Delta t^3 \int_{t^n}^{t^{n+1/2}} \mathrm{d}t\,\|\phi_{tt}\|_{H^2}^2.$$

Taking the inner product of (5.7) with $e^{n+1}+e^n$, we deduce that

$$\frac{1}{\Delta t}(\|e^{n+1}\|^2-\|e^n\|^2)+\frac{1}{2}\|\Delta(e^{n+1}+e^n)\|^2+\frac{S}{2}\|\nabla(e^{n+1}+e^n)\|^2$$

$$=\left(\Delta(e^{n+1}+e^n),f(\bar{\phi}^{n+1/2})-f(\phi(t^{n+1/2}))-S\bar{e}^{n+1/2}+T_2^n\right)+\left((e^{n+1}+e^n),T_1^n\right)$$

$$\leq\frac{1}{2}\|\Delta(e^{n+1}+e^n)\|^2+\frac{1}{2}\|f(\bar{\phi}^{n+1/2})-f(\phi(t^{n+1/2}))-S\bar{e}^{n+1/2}+T_2^n\|^2$$

$$+\frac{1}{2}\|e^n+e^{n+1}\|^2+\frac{1}{2}\|T_1^n\|^2$$

$$\leq\frac{1}{2}\|\Delta(e^{n+1}+e^n)\|^2+\|f(\bar{\phi}^{n+1/2})-f(\phi(t^{n+1/2}))-S\bar{e}^{n+1/2}\|^2+\|T_2^n\|^2$$

$$+(\|e^n\|^2+\|e^{n+1}\|^2)+\frac{1}{2}\|T_1^n\|^2$$

$$\leq\frac{1}{2}\|\Delta(e^{n+1}+e^n)\|^2+2(L^2+S^2)\|\bar{e}^{n+1/2}\|^2+(\|e^n\|^2+\|e^{n+1}\|^2)+\frac{1}{2}\|T_1^n\|^2+\|T_2^n\|^2$$

$$\leq\frac{1}{2}\|\Delta(e^{n+1}+e^n)\|^2+\left(1+4(L^2+S^2)\right)(\|e^{n+1}\|^2+\|e^n\|^2)$$

$$+C\Delta t^3\int_{t^n}^{t^{n+1/2}}\mathrm{d}t\left(\|\phi_{ttt}\|^2+\|\phi_{tt}\|_{H^2}^2+\|\phi_t\|_{H^4}^2\right).$$

In the last inequality, we used (5.6). Then we use the discrete Gronwall's inequality (see [22], pp. 15) to obtain (5.4). □

Remark 5.1. It is a common practice to assume the Lipchitz condition on $f(\phi)$ in Theorem 5.1 [16, 23, 24]. Although it is not directly satisfied by the commonly used form $f(\phi)=(\phi^2-1)\phi$, it has been shown in [25] one can safely truncate $f(\phi)$ for large ϕ) to satisfy the Lipchitz condition without affecting the solution.

Remark 5.2. The results in Theorem 5.1 indicate that, for smooth solutions, the L^2 norm of the numerical solution ϕ^n will remain to be bounded, under the assumptions of Theorem 5.1. However, we are unable to prove the stability directly without the smoothness assumption.

6 Conclusion

We proposed in this paper the stabilized predictor-corrector approach for gradient flows with strong anisotropic systems. The approach leads to schemes which enjoy the following advantages: (i) they are easy to implement as one only needs to solve linear systems with constant coefficients; (ii) they maintain the energy stability of the first-order stabilized scheme; and (iii) they are second order accurate. We numerically validated this approach with three different types of gradient flows with strong anisotropic free energy. And we carried out a rigorous error analysis for the isotropic Cahn-Hilliard equation to show that the stabilized predictor-corrector approach is second-order accurate.

Acknowledgments

References

[1] J. W. Cahn and J. E. Hilliard. Free energy of a nonuniform system. I. interfacial free energy. *The Journal of Chemical Physics*, 28(2):258–267, 1958.

[2] S. M. Allen and J. W. Cahn. A microscopic theory for antiphase boundary motion and its application to antiphase domain coarsening. *Acta Metallurgica*, 27(6):1085–1095, 1979.

[3] F. M. Leslie. Theory of flow phenomena in liquid crystals. *Advances in Liquid Crystals*, 4:1–81, 1979.

[4] M. Doi and S. F. Edwards. *The theory of polymer dynamics*, volume 73. Oxford University Press, 1988.

[5] K. R. Elder, M. Katakowski, M. Haataja, and M. Grant. Modeling elasticity in crystal growth. *Physical Review Letters*, 88(24):245701, 2002.

[6] P. Yue, J. J. Feng, C. Liu, and J. Shen. A diffuse-interface method for simulating two-phase flows of complex fluids. *Journal of Fluid Mechanics*, 515:293–317, 2004.

[7] T. Zhang and Q. Wang. Cahn-Hilliard vs singular Cahn-Hilliard equations in phase field modeling. *Communications in Computational Physics*, 7(2):362, 2010.

[8] S. Dai and Q. Du. Computational studies of coarsening rates for the CahnHilliard equation with phase-dependent diffusion mobility. *Journal of Computational Physics*, 310:85–108, 2016.

[9] X. Yang. Linear, first and second-order, unconditionally energy stable numerical schemes for the phase field model of homopolymer blends. *J. Comput. Phys.*, 327:294–316, 2016.

[10] S. Torabi, J. Lowengrub, A. Voigt, and S. Wise. A new phase-field model for strongly anisotropic systems. *Proceedings of the Royal Society A Mathematical Physical & Engineering Sciences*, 465(2105):1337–1359, 2009.

[11] S. Wise, J. Kim, and J. Lowengrub. Solving the regularized, strongly anisotropic Cahn-Hilliard equation by an adaptive nonlinear multigrid method. *Journal of Computational Physics*, 226(1):414–446, 2007.

[12] F. Chen and J. Shen. Efficient energy stable schemes with spectral discretization in space for anisotropic Cahn-Hilliard systems. *Communications in Computational Physics*, 13(05):1189–1208, 2013.

[13] C. M. Elliott and A. M. Stuart. The global dynamics of discrete semilinear parabolic equations. *SIAM J. Numer. Anal.*, 30(6):1622–1663, 1993.

[14] D. J. Eyre. Unconditionally gradient stable time marching the Cahn-Hilliard equation. In *Computational and mathematical models of microstructural evolution (San Francisco, CA, 1998)*, volume 529 of *Mater. Res. Soc. Sympos. Proc.*, pages 39–46. MRS, Warrendale, PA, 1998.

[15] J. Zhu, L.-Q. Chen, J. Shen, and V. Tikare. Coarsening kinetics from a variable-mobility Cahn-Hilliard equation: Application of a semi-implicit Fourier spectral method. *Physical Review E*, 60(4):3564, 1999.

[16] J. Shen and X. Yang. Numerical approximations of Allen-Cahn and Cahn-Hilliard equations. *Discrete Contin. Dyn. Syst.*, 28(4):1669–1691, 2010.

[17] J. Zhao, X. Yang, Y. Gong, and Q. Wang. A novel linear second order unconditionally energy stable scheme for a hydrodynamic **Q**-tensor model of liquid crystals. *Comput. Methods Appl.*

Mech. Engrg., 318:803–825, 2017.

[18] X. Yang and L. Ju. Linear and unconditionally energy stable schemes for the binary fluid-surfactant phase field model. *Comput. Methods Appl. Mech. Engrg.*, 318:1005–1029, 2017.

[19] X. Yang, J. Zhao, Q. Wang, and J. Shen. Numerical approximations for a three-component Cahn-Hilliard phase-field model based on the invariant energy quadratization method. *Math. Models Methods Appl. Sci.*, 27(11):1993–2030, 2017.

[20] J. Shen, J. Xu, and J. Yang. The scalar auxiliary variable (SAV) approach for gradient flows. *Journal of Computational Physics*, 353:407–416, 2018.

[21] R. Kobayashi. Modeling and numerical simulations of dendritic crystal growth. *Physica D: Nonlinear Phenomena*, 63(3):410–423, 1993.

[22] A. Quarteroni and A. Valli. *Numerical Approximation of Partial Differential Equations*. Springer-Verlag, Berlin, 2008.

[23] D. Kessler, R. H. Nochetto, and A. Schmidt. A posteriori error control for the Allen-Cahn problem: circumventing Gronwall's inequality. *M2AN Math. Model. Numer. Anal.*, 38(1):129–142, 2004.

[24] N. Condette, C. Melcher, and E. Süli. Spectral approximation of pattern-forming nonlinear evolution equations with double-well potentials of quadratic growth. *Math. Comp.*, 80(273):205–223, 2011.

[25] L. A. Caffarelli and N. E. Muler. An L^{∞} bound for solutions of the Cahn-Hilliard equation. *Arch. Rational Mech. Anal.*, 133(2):129–144, 1995.